Investigation of the symmetry-breaking instability in a T-mixer with circular cross section

Claudio Chicchiero,[1] Lorenzo Siconolfi,[2] and Simone Camarri[1, a)]

[1)] *Dipartimento di Ingegneria Civile ed Industriale, Università di Pisa, via G. Caruso 8, 56122 Pisa, Italy*

[2)] *Laboratory of Fluid Mechanics and Instabilities, École Polytechnique Fédérale de Lausanne, 1015 Lausanne, Switzerland*

(Dated: 16 November 2020)

This paper investigates the laminar flow inside a T-mixer composed of three pipes with circular cross-section. The flow enters the mixer symmetrically from the two aligned pipes and leaves the device from the third pipe. In similar devices, but involving rectangular channels instead of pipes, an important regime for mixing has been identified, denoted as engulfment. Despite the symmetries of the flow and of the geometry, engulfment is an asymmetric steady regime which is observed above a critical value (Re_c) of the flow Reynolds number. Conversely, for Reynolds numbers lower than Re_c the flow regime is steady and symmetric, and it is usually denoted as vortex regime. In this paper both the vortex and the engulfment regimes are identified for the considered geometry and they are characterized in detail by dedicated direct numerical simulations (DNSs). Despite an apparent similitude with the behaviour of T-mixers employing rectangular channels, which are the most investigated T-mixers in the literature, substantial differences are observed and highlighted here concerning both regimes, i.e. the vortex and the engulfment ones, and concerning transition between the two. Global stability analysis is finally used in synergy with DNS to investigate the onset of the engulfment regime, which is shown to be related to a symmetry-breaking bifurcation of the vortex regime.

[a)] simone.camarri@unipi.it

I. INTRODUCTION

Micro-mixers are widely used devices and their field of application spreads among several contexts, particularly in chemical and biomedical applications. The main interest for mixers is the enhancement and control of mixing level between two or more reactants, and the objective of their design is to reduce dimensions while keeping high mixing efficiency. This objective is pursued by manipulating the flow inside the mixers since mixing is substantially enhanced by controlling convection at the typical operative conditions. Moreover, mixing is well controllable if the flow remains laminar, and this second characteristic is typical for mixers working at low values of the flow Reynolds number, usually obtained by a combination of small characteristic dimensions (micro-mixers) and low velocities. A wide variety of micro-mixers (or in general mixers working in laminar regime) are described in the literature, and can be divided into *active* and *passive* devices[1,2]. The first class comprises for instance pulsating flow at inlets, local flow control by magnetic fields and, more generally, involves the introduction of energy into the system. Conversely, passive mixers rely on geometry design in order to achieve a good mixing level, for instance by adopting three-dimensional arrangements and by varying the cross section shape.

The interest for passive mixers is based on their robustness and low cost, even though mixing control relies only on fluid dynamic features. Thus, it is important to characterize the flow regimes for different geometries, as it has been done in the literature (see for instance the following review papers: Refs. 1, 3–5); among promising recent configurations we mention passive cross-shaped mixers[6–8]. A wide class of mixers are *T-mixers*; these are characterized by two inlet channels and an outflow one arranged in a T-shaped configuration and are among the most studied mixer configurations in the literature (see for instance Refs. 9–20; see also Ref. 5 for a recent review). Due to their geometrical simplicity, T-mixers are common devices in complex systems and are also employed as junction elements between different branches. Moreover, several geometries have been developed based on the T-mixer shape, as for instance vortex-mixers, which have a gap between the inlet channels[21], and arrow mixers[22], whose inlets form angles different from $\pi/2$ with the outlet channel, as they are generally tilted in comparison with the T-mixer configuration.

By varying the flow Reynolds number, different regimes can be identified in T-mixers with rectangular cross sections. For low Reynolds numbers, the flow is stratified and fluids are seg-

regated. As the Reynolds number is increased, the recirculation bubbles forming at the confluence region between the two entering flows promote the formation of two counter-rotating vortices, each one being folded[23] so that four vortices arranged symmetrically can be found in the outflow channel (*vortex regime*); despite the presence of those vortices the flow remains symmetric and the mixing is caused only by diffusive mechanisms. Above a critical Reynolds number, however, despite the symmetry of the geometry and of the entering flow, the flow changes to an unsymmetrical configuration, where just two co-rotating vortices remain in the outlet channel; this regime is commonly denoted as *engulfment regime*[14,18–20,23–27]. The resulting loss of symmetry promotes a substantial enhancement of mixing level. Further increments of the Reynolds number cause the onset of time-periodic regimes (asymmetric[28] and symmetric[18], respectively) or even chaotic (see also Refs 13, 15–18). These regimes have been largely characterized in the literature and the related flow scenario can be used as a reference for highlighting the peculiarities arising in the flow when cross sections different from the rectangular ones are used.

In order to design a T-mixer which operates in the engulfment regime, it is important to evaluate the critical flow Reynolds number (Re_{cr}) for the onset of this flow regime. The value of Re_{cr} depends on the cross section shape and on the ratio between the areas of the inlet (A_i) and outlet (A_o) channels, which is directly related to the ratio between the inflow and outflow bulk velocity ($\overline{U}_i$ and $\overline{U}_o$, respectively), since $A_o\,\overline{U}_o = 2\,A_i\,\overline{U}_i$ for mass conservation. As concerns this last aspect, it has been observed in the literature that the value of Re_{cr} varies depending on *accelerating* ($\overline{U}_o > \overline{U}_i$ or, equivalently, $A_o < 2\,A_i$) or *decelerating* configurations ($\overline{U}_o < \overline{U}_i$, i.e. $A_o > 2\,A_i$). In particular, the flow acceleration leads to an increase of Re_{cr} if compared to uniform cases ($\overline{U}_o = \overline{U}_i$, $A_o = 2\,A_i$), whereas deceleration decreases Re_{cr}.[26,29].

From what highlighted above, it is important to identify the flow characteristics and the conditions for the onset of the engulfment regime for different cross sections, once the areas ratio A_o/A_i is fixed. To this purpose, there are several studies in the literature focusing on rectangular cross-sections (see for instance Refs 14 and 26). Conversely, despite the fact that the circular cross-section is a paradigmatic shape, easy to build, edge-free and commonly used in channels, T-mixers made by circular channels have not been systematically studied in the literature to the authors' knowledge. Moreover, in contexts very different from T-mixers, such as for instance suddenly expanding circular pipes, a high flow stability has been

observed in comparison with the counterparts employing rectangular cross sections (see for instance Refs. 30 and 31). This fact suggests that even for T-mixers the use of circular cross sections may lead to devices with flow characteristics which are very different from the classical scenario known for rectangular cross sections.

The observations pointed out above justify the need of a detailed investigation of the flow characteristics in circular T-mixers (i.e. composed by circular pipes) in laminar regime. Indeed, on one hand the shape is easy to build and, on the other hand, the only results available in the literature, which moreover do not pertain mixers but simply channels, seem to indicate that the familiar scenario of flow regimes for rectangular mixers cannot be easily estrapolated to circular ones. Despite the fundamental interest in the fluid mechanics of the flow in the considered geometry, a detailed characterization of circular T-mixers can have important impacts in practice, since it is a necessary step for their proper use as devices alternative to the more common rectangular T-mixers. For these reasons the present paper has the objective to explore the flow characteristics in a T-mixer with circular channels, focusing the attention on the first symmetry-breaking bifurcation occurring as the flow Reynolds number is increased. In analogy with the scenario for rectangular T-mixers, the flow after the first symmetry-breaking bifurcation encountered as the flow Reynolds number is increased will be called here "engulfment" and the one preceding the bifurcation will be denoted as "vortex regime". The investigation is mainly carried out numerically by direct numerical simulations (DNSs) and further refined in the identification of the critical conditions by stability analysis. Global stability analysis, which is aimed at identifying and characterizing the instability leading to the engulfment regime, is carried out in analogy with what has been already done in the literature for rectangular T-mixers[22,23,28].

For geometrical reasons, when a circular cross-section is used for the mixer channels, the most natural configuration is an accelerating one with $A_o = A_i$, which grants a geometrically simple matching between the three conduits as they have the same radius, and thus the same width. Keeping this characteristic geometrical aspect fixed, and considering that the section is circular, the counterpart mixer which most resembles the one considered here among those exhaustively investigated in the literature is a T-mixer made by a square cross section with the same area for all the three channels. This counterpart case, whose characteristics are already known and representative for generic rectangular cross sections, is considered here as a reference case, so that the peculiarities of the flow for a circular cross section can be

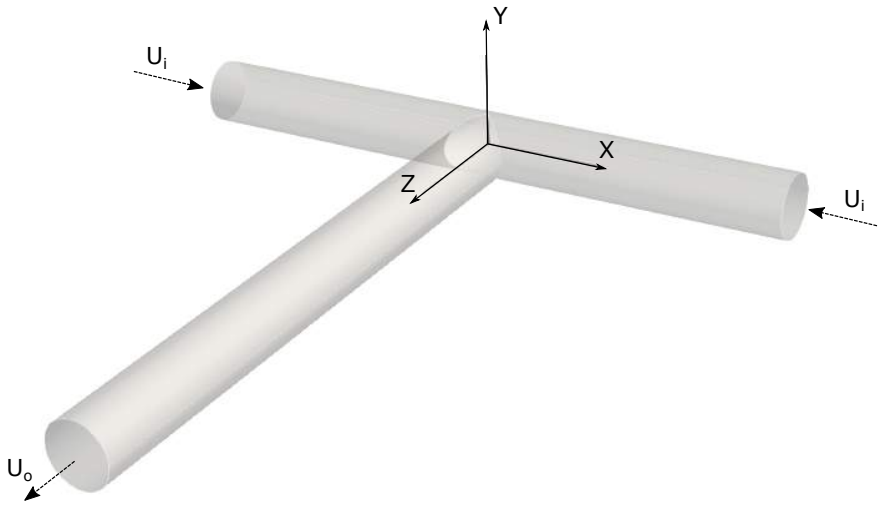

FIG. 1. Geometry configuration and reference system; the direction of the entering (U_i) and leaving U_o flow is indicated using arrows.

highlighted by comparison with this reference case.

As concerns the organization of the paper, sections 2 and 3 present the methodologies used for characterizing the flow and the numerical setup, while section 4 contains a discussion of the results obtained by DNS simulations and by linear stability analysis. Finally, concluding remarks are reported in section 5.

II. FLOW CONFIGURATION AND METHODOLOGY

A. Geometry and flow equations

The configuration considered in the present paper is a T-mixer with a circular cross section, as shown in Figure 1 together with the frame of reference used here. For the sake of brevity, this configuration will be indicated by the label CTM (which stands for Circular T-Mixer). The section diameter D is kept constant along both the inlet and outlet channels, so that the bulk velocity at the outflow is twice the one at inflows for mass conservation ($A_i = A_o$, $\overline{U}_o = 2\,\overline{U}_i$). The same fluid at the same thermodynamic conditions enters from the two inlets, i.e. we consider the case working with only one homogeneous fluid.

All dimensions are normalised using the diameter D of the cross section as the reference length, while the reference velocity is the bulk velocity at inflow channels $\overline{U}_i$. The flow dynamics is described by the incompressible Navier-Stokes equations in non-dimensional

form:

$$\begin{aligned} &\nabla \cdot \mathbf{U} = 0 \quad , \\ &\frac{\partial \mathbf{U}}{\partial t} + \mathbf{U} \cdot \nabla \mathbf{U} + \nabla P - \frac{1}{Re} \Delta \mathbf{U} = 0 \quad , \end{aligned} \tag{1}$$

where $\mathbf{U} = (U, V, W)$ is the velocity field vector and P the non-dimensional pressure.

The Reynolds number Re is defined as

$$Re = \frac{\overline{U}_i D}{\nu} \quad , \tag{2}$$

where $\overline{U}_i$ is the bulk velocity at the inlet (i.e. the average of the inlet velocity profile), D the diameter of cross section and ν the kinematic viscosity.

In order to understand the effect of having a circular section in comparison with the scenario which is more familiar from the literature, a T-mixer with a square cross section (and $A_o = A_i$) has been considered as a test case for comparison. In the following this mixer configuration will be indicated by the label STM (standing for Square T-Mixer). In the STM case we consider as the reference length for normalization the hydraulic diameter D_h defined as

$$D_h = \frac{4A_s}{P_s} \quad , \tag{3}$$

where P_s and A_s represent the perimeter and area of the cross section, respectively. We remark that for the square section considered here the hydraulic diameter corresponds to the lenght L of the section sides ($D_h = L$).

The flow characteristics in the STM has been investigated in details in Ref. 26. We remark that in Ref. 26 the selected reference velocity for normalization is the bulk velocity at the outflow $\overline{U}_o$, thus the Reynolds number for the STM, $Re_{s,o}$, is defined in Ref. 26 as:

$$Re_{s,o} = \frac{\overline{U}_o D_h}{\nu} \quad . \tag{4}$$

The critical flow conditions for the onset of the engulfment regime in a square mixer has been identified in Ref. 26 and the corresponding critical Reynolds number is assessed to be $Re_{s,o} \simeq 270$. As a final remark, it has to be taken into account that the Reynolds number referred to the outflow bulk velocity is twice the one based on bulk velocity (Eq. 5) when $A_i = A_o$, as it is the case here, and in the present work we have chosen the inlet bulk velocity as the reference one. Thus, hereafter the critical Reynolds number for the STM based on the inlet bulk velocity will be indicated as Re_s and its critical value for the onset of engulfment

for a STM is $(Re_s)_{cr} \simeq 135$, in order to preserve the same normalization adopted here for the CTM, i.e.

$$Re_{s,o} = \frac{\overline{U}_o D_h}{\nu} = \frac{2\overline{U}_i D_h}{\nu} = 2Re_s \quad . \tag{5}$$

B. Stability analysis

The onset of the instability leading to the engulfment is also investigated here through linear stability and normal-mode analysis. In the following, the basic theory is briefly recalled. The flow $\mathbf{U}$ is decomposed in two contributions:

$$\begin{aligned} \mathbf{U} &= \mathbf{U_b} + \mathbf{u} \quad , \\ P &= P_b + p \quad . \end{aligned} \tag{6}$$

The first is the baseflow $(\mathbf{U_b}, P_b)$, which is the steady solution of NS equations (Eq.1), while the second is the perturbation field $(\mathbf{u}, p)$. When studying the engulfment instability, $(\mathbf{U_b}, P_b)$ is the flow solution which respects the same symmetries of the geometry, i.e. the flow solution in the vortex regime. By substituting the decomposition in Eq. (1) and neglecting non-linear terms in the perturbation field, the equations governing the linearised perturbation dynamics are obtained. The perturbation $(\mathbf{u}, p)$ is chosen in the modal form $(\mathbf{u}, p) = [\hat{\mathbf{u}}(x, y, z), \hat{p}] \exp(\sigma t)$, where $\sigma = \lambda + i\,\omega$ is complex-valued, i is the imaginary unit and both λ and ω are real numbers. According to this notation, the resulting eigenfunction problem to be solved for inspecting stability of the baseflow is

$$\begin{aligned} &\nabla \cdot \hat{\mathbf{u}} = 0 \quad , \\ &\sigma \hat{\mathbf{u}} + \hat{\mathbf{u}} \cdot \nabla \mathbf{U_b} + \mathbf{U_b} \cdot \nabla \hat{\mathbf{u}} + \nabla \hat{p} - \frac{1}{Re} \Delta \hat{\mathbf{u}} = 0 \quad . \end{aligned} \tag{7}$$

Homogeneous Dirichlet boundary conditions are imposed for the velocity perturbation at inflow boundaries and on solid walls, i.e. $\hat{\mathbf{u}} = 0$, while a stress-free condition is applied at the outflow boundary. The baseflow $(\mathbf{U_b}, P_b)$ is linearly unstable if there is at least one non-trivial solution of Eq. (7) for which $\lambda > 0$. In the opposite case, a generic small perturbation of the baseflow asymptotically decays in time and the flow is thus linearly stable. When only one unstable eigenvalue is identified and the instability is supercritical, as it is the case here, the associated eigenmode $(\mathbf{u}, p)$ is also representative of the path followed by the flow to depart from the baseflow state in the initial stages of the instability, i.e. when perturbation

is still small so that non-linearities do not significantly affect its dynamics. Moreover, still when in slight supercritical conditions, in many cases the shape of the perturbation $(\mathbf{u}, p)$ may be at least representative of that of the fully saturated instability as well. For more details on the subject we refer for instance to Refs. 32 and 33.

III. NUMERICAL TOOLS

A. Direct Numerical Simulations

DNS simulations have been carried out by using the spectral element code Nek5000 (see the following url: *https://nek5000.mcs.anl.gov* for more details). Inlet channels span in the range $x = [-7\,D, +7\,D]$, i.e. each one is $7\,D$ long, while the length of the outlet pipe is equal to $25\,D$. This length has been selected according to the indications provided in previous works on mixers[23,28] and is chosen in order to completely describe the development of vortical structures along the outlet channel. The Hagen-Poiseuille velocity profile is imposed at inflow boundaries, no-slip condition at the walls and a stress free condition at the outflow boundary.

In order to obtain results that are grid-independent, different p-refinement levels have been tested, not shown here for the sake of brevity. The results reported hereafter are obtained by using a multiblock structured grid composed by 26640 spectral elements. In order to avoid spurious pressure modes, the P_N/P_{N-2} approximation has been adopted, with the degree of base polynomials N equal to $N = 6$. Simulations have been advanced in time with a Courant-Friedrichs-Lewy (CFL) number not higher than 0.5, and steady solutions have been identified by advancing the simulations in time until the L_2-norm of velocity residuals became less than a prescribed value (10^{-6} in our case).

In order to qualitatively assess the mixing behaviour of the mixer, a passive scalar is injected from one inlet channel, whose diffusivity coefficient κ has been set to the lowest allowable value for numerical stability without any artificial stabilization ($\kappa = 3 \cdot 10^{-4}$), thus minimizing diffusive mechanism and trying to mainly highlighting the mixing given by convective phenomena.

B. Stability analysis

The stability analysis was carried out by using ad-hoc tools implemented in Nek5000, already validated in previous works[22,23,28,34]. The algorithm is based on Arnoldi-Krylov decomposition along with a Gram-Schmidt orthogonalization and allows the approximation of the leading eigenvalues of the system. Starting from an initial perturbation generated randomly, the application of the system matrix is approximated using the Linearized Navier Stokes (LNS) solver already implemented in Nek5000, in order to obtain a Krylov basis $\mathcal{K}$ and a Hessenberg matrix $\mathcal{H}$. Once $\mathcal{H}$ is obtained, its eigenvalues can be evaluated directly using LAPACK libraries[35]. The eigenvalues of the original system can be successively computed as:

$$\sigma = \frac{\log \Sigma}{\Delta t} \quad , \tag{8}$$

where Σ are the eigenvalues of the Hessenberg matrix and Δt is the sample time. The size of the Krylov subspace has been chosen heuristically and on the basis of dedicated tests. The sample time has been fixed so as to have negligible effects on the leading eigenvalue. An extensive description of the algorithm can be found in Ref. 36.

IV. RESULTS

As for the square T-mixer (STM), the flow in the circular T-mixer (CTM) has the same reflectional symmetries of the geometry provided that the flow Reynolds number is sufficiently low. As Re is increased, the symmetric configuration undergoes an instability leading the flow to a steady unsymmetric regime. In analogy with the literature on STM, besides the substantial differences with the CTM that are highlighted in the following, we will denote here as "vortex" and "engulfment" regimes the symmetric subcritical and the unsymmetric supercritical flow regimes observed in the CTM. Without entering for the moment into the details of the characteristics of such flow regimes in the CTM, as they will be discussed later, we now focus only on the flow conditions (i.e. on the flow Reynolds number, this being the only free parameter governing the flow) for their onset and for the transition between one state to the other. This aspect has been investigated here firstly by DNS.

Figure 2 recaps the simulated flows and the corresponding regimes, i.e. the vortex and the engulfment regimes, found by DNS. As concisely shown in figure 2, the critical Reynolds

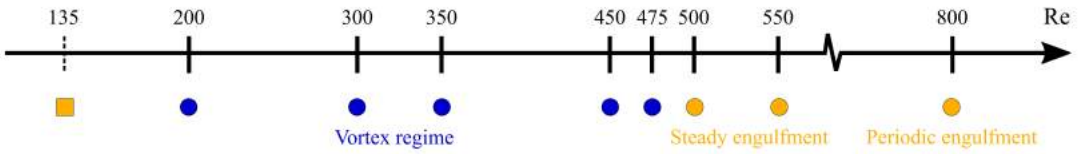

FIG. 2. Simulations carried out by spanning the flow Reynolds number and corresponding flow regimes identified for the CTM. The square marker denotes the critical Reynolds number for the STM, as reported in Ref. 26.

number Re_{cr} for the transition between the vortex and the engulfment regimes is estimated to be in the interval $475 \leq Re_{cr} \leq 490$, and this result is confirmed by stability analysis as shown in the following. Hysteresis in the onset of the engulfment regime has been excluded by dedicated DNS simulations, which have been carried out by progressively increasing and decreasing the Reynolds number across Re_{cr}, thus confirming the supecritical nature of the symmetry-breaking bifurcation leading to the engulfment in CTM.

As mentioned in Ref. 26, the flow acceleration in the outlet channel involves higher critical Reynolds numbers with respect to decelerating T-mixers. However, it has to be noted that the critical Reynolds number for the CTM is definitely higher (about than 3.5 times larger) than the one of the STM ($Re_{cr,s} = 135$), showing that the vortex regime in the CTM still exists but at definitely larger bulk velocities than in the STM when the same working fluid is employed. This result alone already highlights the surprisingly large difference existing between the two mixers.

As concerns the flow configuration that is established after the engulfment regime, since this is not the focus of the present paper, only one simulation was carried out for $Re = 800$, at which a periodic flow regime is observed. In particular, at $Re = 800$ the flow in the CTM is in an unsymmetrical periodic regime, i.e. a flow which is periodically oscillating around a configuration which does not respect the symmetries of the geometry, as also observed in T-mixers with rectangular cross sections[27,28]. The unsymmetrical periodic regime is not investigated any further in this paper.

In the next sections, we describe in details the vortex regime at values of Re in the range $150 < Re < 475$. Then, the flow is characterised as the Re is either decreased (vortex

regime at lower Reynolds numbers) or increased (engulfment regime). Lastly, the results of the linear stability analysis are discussed.

A. Flow in the vortex regime for $150 \leq Re \leq 475$

The vortex regime is the flow configuration with the same reflectional symmetries of the geometry itself observed in CTM for $Re \leq 475$. In order to discuss the characteristics of the vortex regime in CTM we focus for the moment on the flow simulated for $Re = 450$, i.e. in slightly subcritical conditions for the onset of the engulfment regime. The characteristics of the vortex regime at lower values of the flow Reynolds number, specifically for $Re < 150$, will be illustrated in a successive dedicated subsection.

By definition, the flow field at the considered conditions is invariant for reflections with respect to both $x - z$ ($y = 0$) and $y - z$ ($x = 0$) planes. The flow in the inlet pipes is a developed Poiseuille flow (unidirectional and parabolic in the radial direction) and maintains this aspect up to a x-coordinate approximately equal to $|x| = 1.0$, where the velocity profile starts to significantly deviate from the Poiseuille one (parabolic in the radial direction) due to the pressure field induced by the flow at the confluence region of the three pipes. In the confluence region two opposing flows coming from the inlet pipes meet and enter the outlet pipe.

The first important aspect is that, as for the STM, a separation region forms on the top wall, i.e. the portion of wall of the mixer in the confluence region that is opposite to the outlet pipe. The shape of this separation region is reported in figure 3(b) in perspective view and in 3(a) and 3(c) for $x - y$ and $x - z$ views. In figure 3 the surface delimiting separation has been identified based on the sign of the velocity x-component; for this reason a small portion is not included (see label "E" in figure 3(a)) due to a small secondary recirculation region denoted as "R2" in figure 3(c). As evident by figure 3(c), the separation region is elongated towards the inlet pipes and is made by three main vortices, a dominant one denoted as R1 and two definitely weaker secondary vortices, R2 and R3. All of them are contained in the separation region, whose boundary with the external unseparated flow is shown in both figures 3(b) and (c).

As already highlighted, the separation region is made by two main counter-rotating vortices (only one is reported in figure 3, i.e. that in the region $x \geq 0$) which are related to

the strongest recirculation region inside the separation region (R1), and are specular with respect to the plane $x = 0$. The so-formed vortices, which collect part of the vorticity generated at the walls in the incoming flow and whose maximum normalized vorticity is of the order of 55 at $Re = 450$, elongate toward the outlet pipe while remaining in a symmetric arrangement. One of the two is visualized in figure 3 by streamlines of the flow generated starting from proper points inside the vortex itself. This visualization, which of course has been verified to agree with the λ_2 criterion[37], has been chosen here instead of the iso-surface of the λ_2 scalar field as it is clearer and sharper for the case at issue, and moreover allows us to track different vortices as will be shown later. As shown in figure 3, each vortex formed in the separation region near the top walls originates two "legs" which are convected by the flow in the outlet pipe. Figure 3 puts in evidence their shape in the top portion of the mixer considered in the figure. Even if not shown, the identified vortices are subjected initially, i.e. when entering the outlet pipe, to a positive stretching due to the accelerating velocity gradients of the flow. They experience a compression (which is opposite to stretching) only further downstream in the outlet channel, as discussed later since this aspect plays a role in their successive development.

At the confluence region, almost aligned with the axis of the inlet pipes, a region of high pressure forms, with its maximum at $x = 0$, and pressure quickly drops towards the outlet pipe in the confluence region, i.e. for $z > 0.3$. In quantitative terms, at $Re = 450$ the normalized pressure drop from $z = 0$ to $z = 1$ is equal to $\Delta p \simeq -5.1$, which is a large variation considering that the pressure drop in the outlet channel from $z = 1$ to $z = 10$ is $\Delta p \simeq -3.0$. As a consequence of the pressure gradient at the entrance of the outlet pipe, the flow is markedly accelerated towards the outlet pipe. Moreover, due to the geometry of the device, a curved and sharp edge is present between each inlet pipe and the outlet one. As the edge is a sharp corner, it induces flow separation at the entrance of the outlet pipe. This separation region, denoted in the following with the label RL so as to differentiate it from the separation near the top wall of the mixer (labelled as RH), is visualized in three dedicated detailed views reported in subfigures 4(b-d), and is plotted together with RH in figure 4(a). In particular, the surface denoted as RL in figure 4 represents recirculation in the z-direction, which is the direction of the main stream leaving the confluence region.

At difference with the STM, where the edge between the pipes is sharp but straight, and does not lead to the formation of vortices, the peculiar circular shape in the CTM promotes

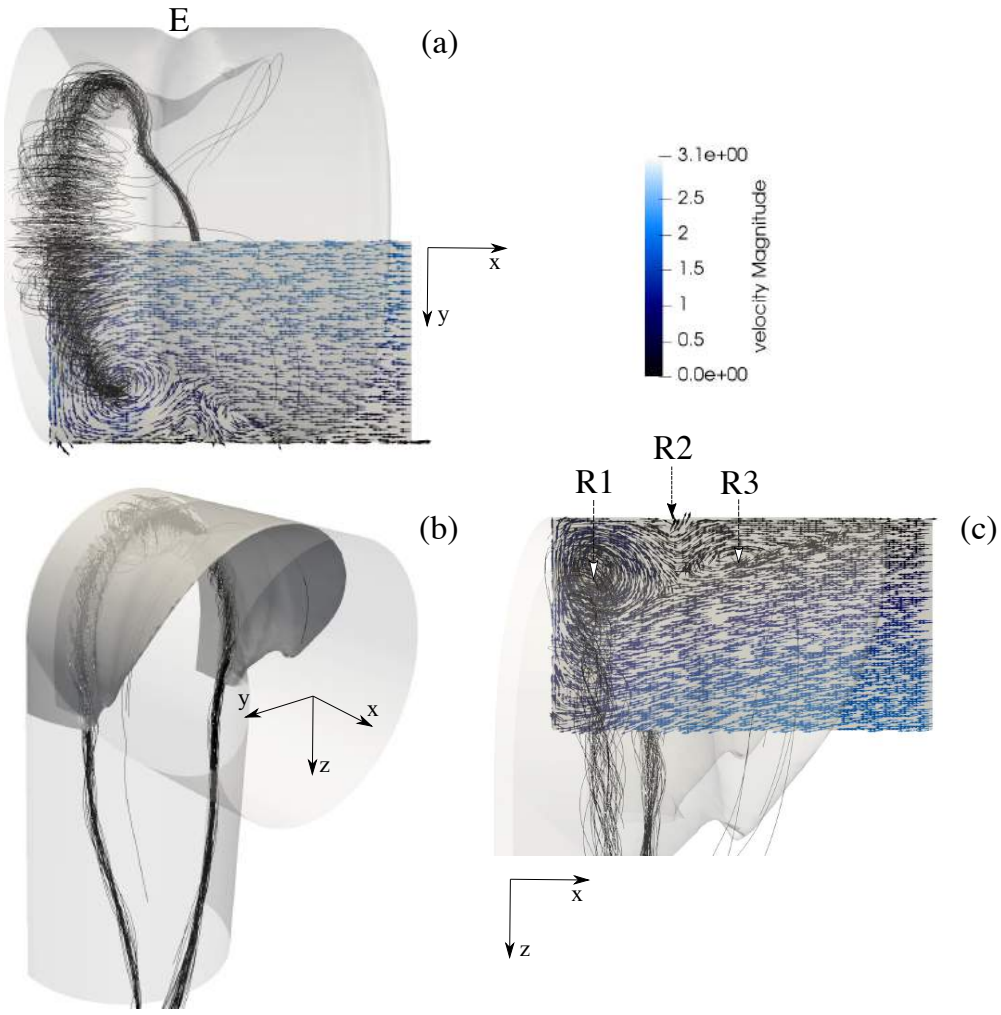

FIG. 3. Flow field in the vortex regime at $Re = 450$: separation region on the top wall of the mixer, visualized by a transparent grey surface darker than the mixer walls, also shown for clarity, and associated vortex visualized by means of streamlines: (b) perspective view, (a) $x-y$ view and (c) $x-z$ view; we report also in-plane vectors indicating the velocity direction at sections (a) $y = 0$ and (c) $z = 0$; in-plane color contours indicate the in-plane velocity magnitude; only half plots are presented as the flow has two reflectional symmetries.

the formation of two strong counter-rotating vortices, denoted as L1 and L2 in figure 4, delimiting the RL region. Concerning intensity, we found that the maximum intensity of the normalized vorticity in L1 and L2 in figure is approximately equal to 55 at $Re = 450$. Their initial formation stage in connection with RL is illustrated in figure 4(b), while their shape along the outlet channel can be seen in figure 4(a), where they are represented by darker color so as to differentiate them from the vortices coming from the top, i.e. H1 and H2.

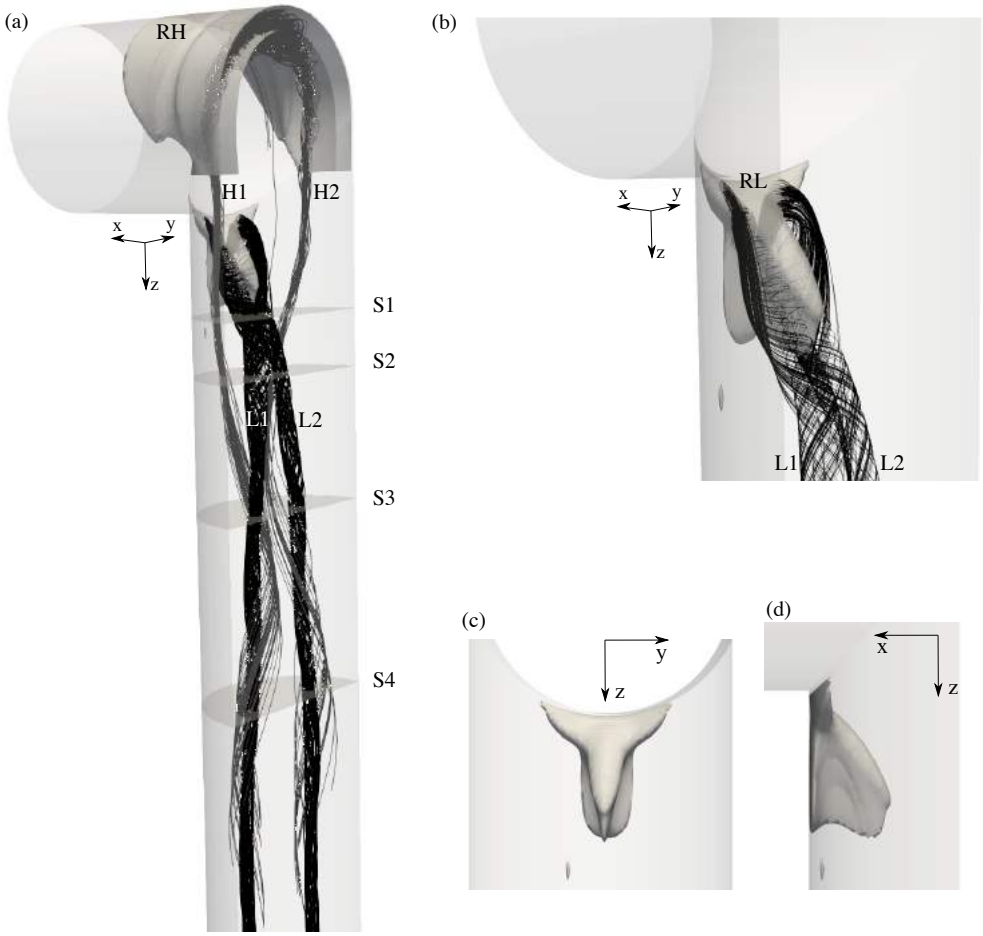

FIG. 4. Flow field in the vortex regime at $Re = 450$: separation regions on the top wall of the mixer (RH) and at the intersection between the inlet and the outlet pipes (RL), visualized by a transparent grey surface darker than the mixer walls, also shown for clarity; vortices originating at RL are visualized using streamlines; the vortex legs H1 and H2, in lighter color, originate from RH while the legs L1 and L2 from RL; R1 and L1 are co-rotating, the same applies for R2 and L2, while R1 and R2 (or equivalently L1 and L2) are counter-rotating; subfigures (b), (c) and (d) are three detailed views of RL, (b) in perspective, (c) is a $y - z$ view and (d) a $x - z$ view.

As for H1 and H2, also L1 and L2 have been identified using properly generated streamlines, and the derived shapes agree with the λ_2 criterion (not shown here in order to not further complicate figure 4). Vortices analogous to L1 and L2 can also be found in the STM, but they are extremely weak and play unsignificant role in the flow dynamics. Conversely, the flow dynamics of the CTM is fundamentally governed by the interplay between H1, H2, L1 and L2, all of which are of comparable amplitude, as it will be illustrated in the following.

A first effect of L1 and L2 is the shape of the RL region. Indeed, due to the sign of their vorticity and to the direction of the velocity they induce on themselves, L1 and L2 initially travel towards the centerline of the outlet pipe, thus determining the peculiar shape of RL which is thin and elongated towards the center of the outlet pipe. Considering mass conservation and the fact that the flow is reversed (with respect to z) inside RL and slow in its near-wake, it can be deduced that the flow at z-sections in proximity of RL is strongly accelerated near the centerline of the outlet pipe. Indeed, the z-component of velocity on the outlet axis passes from a value approximately equal to 2.0 at the entrance of the outlet pipe to the value 3.2 at $z \simeq 1$, i.e. just after RL, where it reaches its maximum value. This aspect, together with the peculiar distribution of the z-velocity over z-sections, is shown for section S1 in figure 5(a) (see figure 4(a) for identifying the position of section S1). Figure 5 shows that the recirculating region RL leaves a wake of low velocity in the z-direction which contains the two vortices L1 and L2 and extends towards the centerline of the outlet pipe. Consequently, since the region characterized by low z-velocity has an important area in comparison with the whole section, some areas of section S1 are characterized by values of z-velocity reaching peaks of 3.2 (we remind that 2.0 is the value which, if uniform on the section, grants mass conservation in the outlet pipe). Progressing further in the outlet pipe up to section S2, see figure 5(b), vortices L1 and L2 are closer to the symmetry plane $x = 0$ due to their self-induced velocities, while vortices H1 and H2 coming from RH have a deformed core because they approach a region with a high in-plane velocity shear. In this region, moreover, H1 and H2 are subjected to an adverse axial velocity gradient, i.e. to vortex compression. As a result, vortices H1 and H2 disappear further downstream of S2 as the in-plane shear becomes dominant over the rotational part of the velocity field. This is highlighted by both the λ_2 criterion, whose contours identifying vortices are reported in figure 5 showing that H1 and H2 disappear after section S2 (see subfigures (c) and (d)), and by the streamlines in figure 4(a) where the distribution of streamlines in H1 and H2 after section S2 clearly shows a spreading and a sudden disappearance of the core of the vortices. We underline that a vortex disappears in our viewpoint when it cannot be identified any more by the vortex identification criterion selected, in this case the λ_2 criterion, due to the prevalence of shear over rotation in the kinematic analysis of the velocity field. However, vorticity carried out by the identified vortices remains in the flow field, as it is solenoidal, undergoing convection, diffusion and stretching/tilting. Considering the relative positions

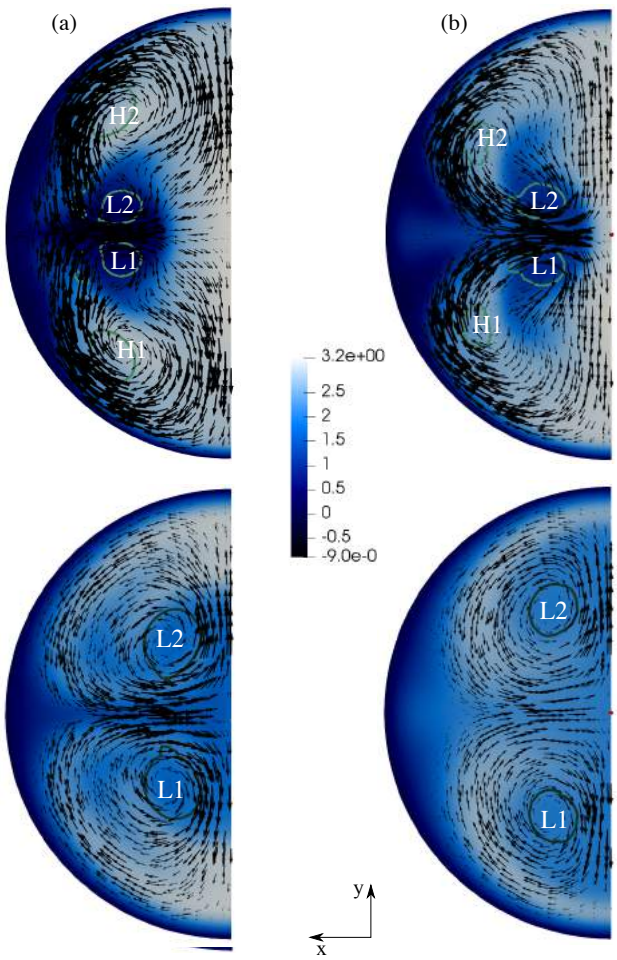

FIG. 5. Flow field in the vortex regime at $Re = 450$; flow at sections (a) z=1.0 (S1 in figure 4(a)), (b) z=1.3 (S2), (c) z=2.0 (S3) and (d) z=3.0 (S4): vectors indicate the in-plane velocity field (vector lengths are scaled with the local amplitude of the in-plane velocity) and the coloured contours indicate the z-component of velocity; for labels H1, H2, L1 and L2 please refer to figure 4

.

of vortices and their sign, and considering that at the selected Reynolds number convection is dominant over diffusion, it is probable that vorticity from H1 (H2) merges with L1 (L2) once the vortices H1 and H2 have disappeared in the sense specified above. Conversely to H1 and H2, vortices L1 and L2 persist, as shown both in figure 4(a) and in figures 5 (c-d). Even if not shown, it has been also observed that vortices L1 and L2 are continuously subjected to a positive stretching, as can be qualitatively deduced in figures 5 by observing that the z-component of velocity where L1 and L2 are located is progressively increasing when proceeding downstream in the outlet pipe. These elements make vortices L1 and L2

stable and dominant, so that at a sufficient distance from the confluence region they are the only vortices that are present (see for instance figures 5 (c-d)), while the z-component of velocity is progressively more uniform across the section tending asymptotically to a parabolic distribution (here the outlet pipe is too short to demonstrate this fact). As a net result, the secondary flow in the outlet pipe at a sufficient distance from the confluence region resembles that of the STM and of rectangular T-mixers in general since it is dominated by four counter-rotating vortices organized symmetrically along the symmetry planes of the geometry. However, as shown here, the origin of these vortices in the two kinds of mixers is completely different; indeed in the CTM the vortices originate at the sharp edges between the three pipes in the confluence region while in the STM they come from the separation region near the top walls of the mixer.

Despite this substantial difference, the vortex regimes in the CTM and in the STM at first sight look very similar and in both cases, due to symmetries, the flows coming from the two inlet pipes are always separated in terms of convection, i.e. the plane $x = 0$ is a stream-surface for the flow. Consequently, mixing between the two flows is driven by diffusion.

B. Flow in the vortex regime at $25 \leq Re < 150$

As discussed above, the vortex regime in CTM at $Re = 450$ is dominated by the mutual interaction between two types of vortical structures, i.e. the vortices originating in the RH region (H1 ad H2 in figure 4) and those forming in RL region (L1 ad L2 in figure 4). The flow scenario identified at $Re = 450$ in subsection IV A remains substantially unchanged when the value of Re is decreased down to $Re = 150$. When Re is further decreased, the separation region RL rapidly shrinks, and disappears for Re in the range $50 < Re < 100$. Most importantly, vortices originating in RL also weaken and disappear even before the RL region; for instance, in our DNSs they are absent already for $Re \leq 125$. It is evident that, as a consequence, a flow scenario is observed for sufficently low Re which differs from that identified at $Re \geq 150$. In particular, the flow at $Re < 150$ still respects the same reflectional symmetries of the geometry but the flow dynamics is dominated by different systems of vortical structures. In the range $50 \leq Re \leq 125$ the vortices originating in the RH regions are still present, although they

are progressively weaker as Re is decreased. At the same time another system of vortices can be identified, which originates from the secondary flow forming in the inlet channels near the confluence region between the three pipes. One among the four vortices of this system, which are symmetrically arranged due to the flow symmetry, is shown in figure 6(a) at $Re = 100$ with the label "SV". As shown in the figure, vortex SV is initially very weak but gains intensity due to intense vortex stretching when entering the outlet pipe. As shown in the figure, also the vortices (only one vortex is shown in the figure) originating in RH are present but they are weak and placed in a high-shear region in the outlet pipe, so that they do not play any significant role. Indeed, vortices dominating the secondary flow in the outflow pipe are those originating from the secondary flow in the inlet pipes, i.e. SV, as shown in figure 6(a). This is even clearer at $Re = 25$, as shown in figure 6(b), where the recirculation region RH disappears together with the associated vortices. This last aspect is put in evidence in the insert of figure 6(b) proposing a zoomed view of the velocity field near the surface of the mixer where the RH region is usually positioned. Thus, at $Re = 25$ only vortices SV are present and, as for $Re = 100$, they dominate the secondary flow observed in the outlet pipe. Note that vortices SV can be found also for $Re > 150$ but they are extremely weak in comparison with the other two systems of vortices and thus they do not play any role in the flow.

Concerning the transition between the two main scenarios outlined here, which happens approximately in the range $100 < Re < 150$, this is smooth as observed by DNS and not related to an abrupt change which might indicate a bifurcation.

C. Flow in the engulfment regime

When the Reynolds number exceeds the value Re_{cr} (we remind that $475 \leq Re_{cr} \leq 490$, see also figure 2) the flow undergoes a bifurcation and sets itself into a steady asymmetric regime which is denoted here as engulfment. Despite the two reflectional symmetries of the geometry are broken in the engulfment regime, nevertheless the flow field is symmetric by a rotation of an angle equal to π around the symmetry axis of the outlet pipe or, equivalently, by two subsequent reflections about the $y-z$ and the $x-z$ planes. This aspect is common to the engulfment observed also in the STM and in rectangular T-mixers in general. Conversely, one among the peculiarities of the engulfment in the CTM is that the flow remains practically

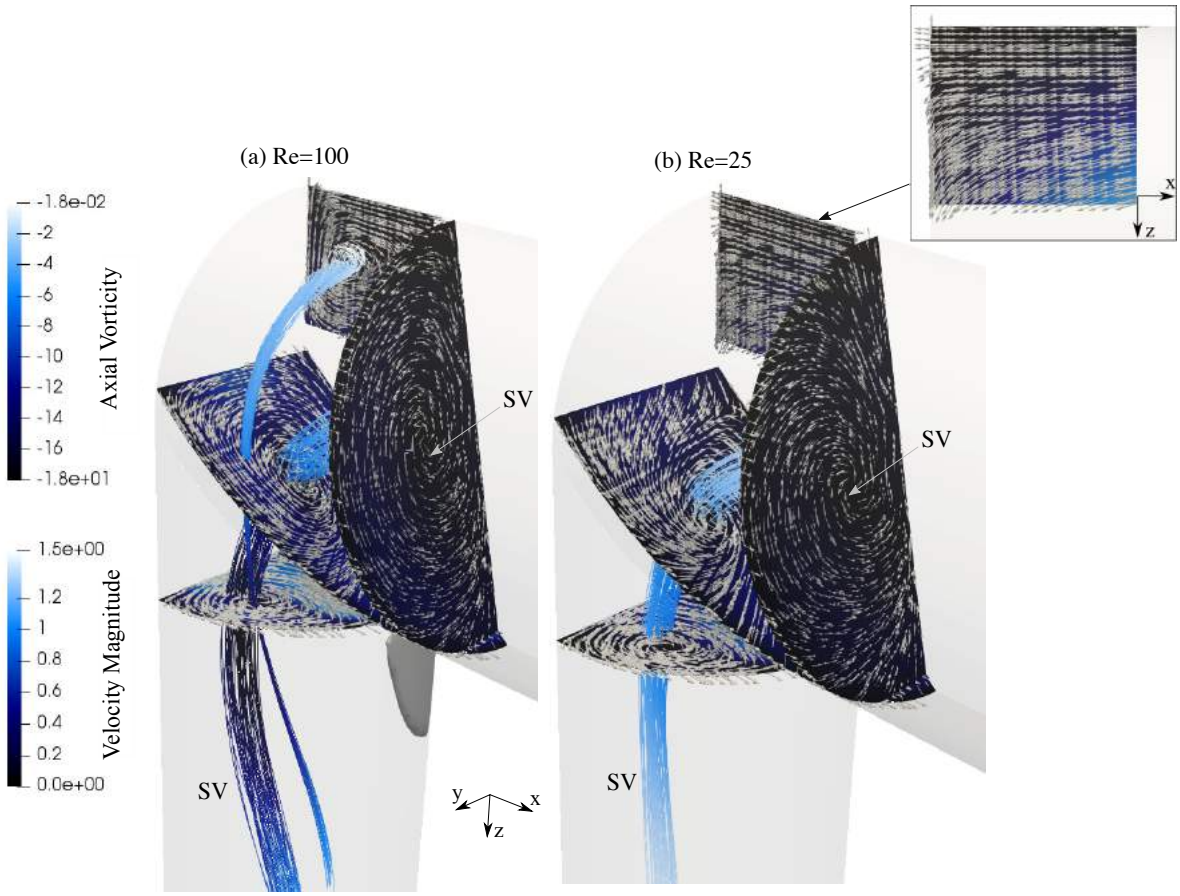

FIG. 6. Flow field in the vortex regime at (a) $Re = 100$ and (b) $Re = 25$; sections show the in-plane velocity direction by vectors and magnitude by color contour, while the streamlines identifying vortices are coloured according to the axial vorticity (for the sign convention see the rotation direction that can be desumed by the velocity arrows).

symmetric in the inlet pipes and in the confluence region, at least for $z \leq 0.9$. At difference, in the STM the asymmetry is very evident already in the confluence region, where the vortices forming on the top wall of the mixer tilt and originate two strong and two weak legs entering the outlet mixer, and the two strong ones, which are also co-rotating, dominate the flow dynamics in the outlet pipe driving mixing by convection. In the CTM the flow remains practically symmetric also in the very first part of the outlet pipe until the two couples of counter-rotating vortices form from the sharp edges in proximity of the RL region. One couple of counter-rotating vortices, namely L1 and L2, are visualized in figure 7(a) and (b) by properly generated streamlines in lighter color. Only a couple is reported because the other couple evolves symmetrically as explained above (rotational symmetry by an angle π around

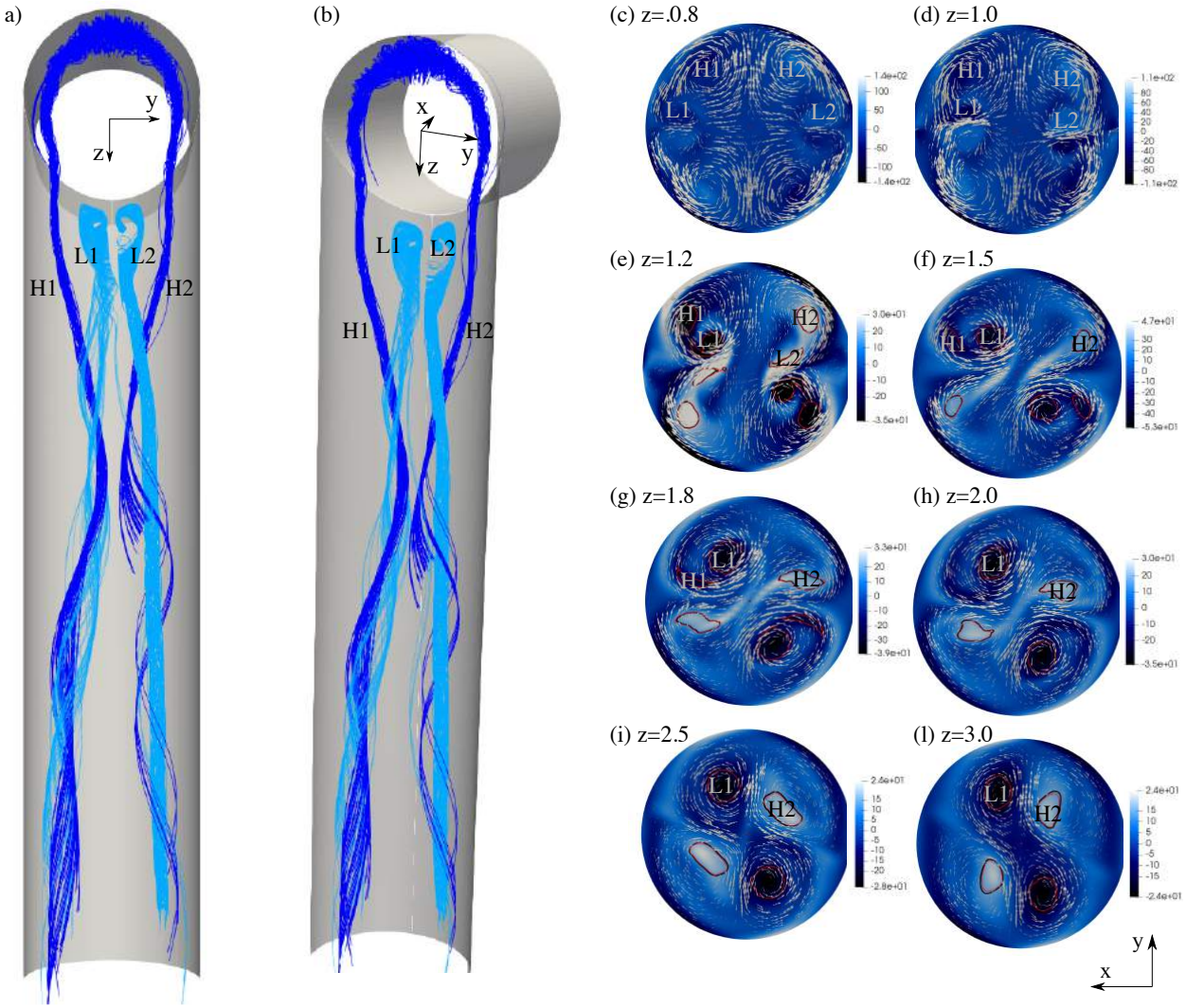

FIG. 7. Flow field in the engulfment regime at $Re = 550$: (a)-(b) perspective views of the vortices originating from the RH (H1 and H2, darker color) and the RL (L1 and L2, lighter color) regions; (c)-(l) z-sections of the flow showing the in-plane velocity (vectors) and the z-component of vorticity.

the z-axis). As vortices L1 and L2 travel towards the outlet channel while gaining intensity due to vortex stretching, the two vortices of each couple start to develop asymmetrically, and as a first consequence the RL separation regions loose their symmetry with respect to the $x - z$ plane, as shown in figure 8 where this is represented by a grey surface in perspective (a), in $y - z$ (b) and in $x - z$ (c) views. Comparing the flow features shown in figure 8 with the equivalent ones in figure 4 for the vortex regime, it is evident that the RL region is now asymmetric as the vortices L1 and L2 which are associated with it, visualized both in figure 7 and in figure 8. Also the four vortices forming in the RH region,

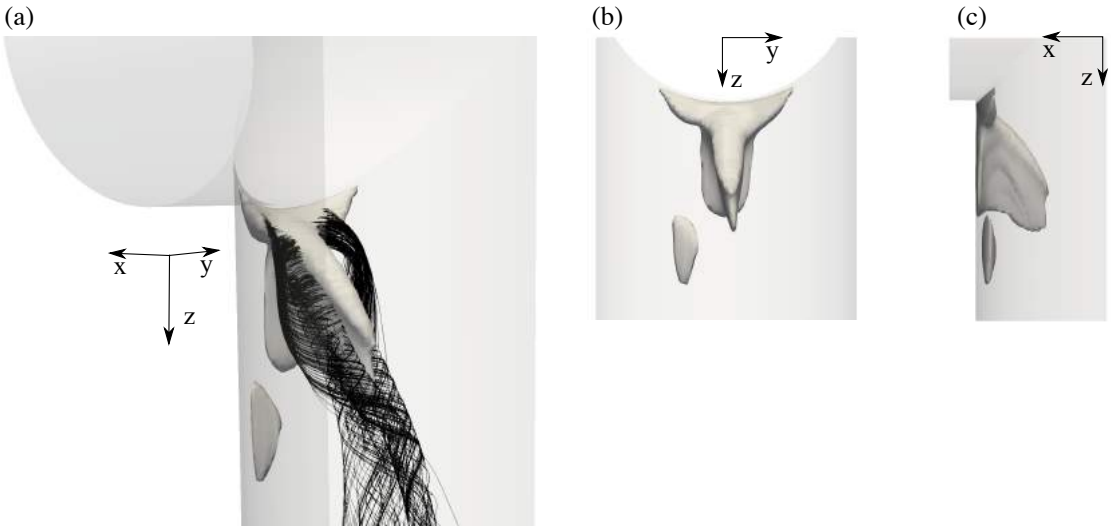

FIG. 8. Flow field in the engulfment regime at $Re = 550$: separation region from the sharp edges in the CTM in the engulfment regime ($Re = 550$), RL, visualized by a transparent grey surface darker than the mixer walls, also shown for clarity; associated vortices are visualized by means of streamlines in (a): (a) perspective view, (b) $x - y$ view and (c) $x - z$ view.

two of which are reported in figure 7(a) by proper streamlines in darker colours (see labels H1 and H2), start to be asymmetric as a consequence of the interaction with L1 and L2. This fact can be appreciated in figures 7(c)-(d) where the vortices are reported together with the in-plane velocity field (vectors) and the z-component of vorticity (color contours) at selected z-sections. Besides the increasing asymmetry of the configuration, the referenced figures and especially subfigure 7(d) show that couples (H1,L1) and (H2,L2) interact as in the vortex regime. However, due to the asymmetry highlighted above, the dynamics of the two couples is different. This is well highlighted by following sequentially subfigures 7(e)-(h), which contains the same information of the previously discussed subfigures but refer to slices taken at increasing values of z. The sequence of subfigures shows that, as concerns the couple (H1,L1), its development along the outlet pipe is similar to what observed in the vortex regime. In particular, vortex H1 moves in a region with high in-plane shear which becomes dominant deforming the vortex core of H1 until the vortex disappears. This is confirmed by the representative iso-contour of the λ_2 criterion also reported in the figures as a red/black line. Surprisingly, the dynamics of the couple (H2,L2) is different. Indeed in this case it is vortex L2 to move in a region of high in-plane shear and to disappear in the sense already specified in the discussion of the vortex regime. As a consequence, for $z \geq 2$

only vortex H2 remains from couple (H2,L2), i.e. a vortex which originates from the RH region, while only vortex L1 remains of the couple (H1,L1), i.e. a vortex originating from the RL region. Inspecting subfigure 7(e-g) it is probable that the main part of vorticity initially carried out by vortices H1 and L2 is collected by vortices L2 and H1, respectively. Both L1 and H2 have similar amplitude, even if amplitude of L1 is slightly higher, and L1 and H2 are counter-rotating. We remind that we are discussing the dynamics of the flow in the outlet pipe for $y \geq 0$, as the flow in $y \leq 0$ is the same but rotated by an angle π around the z-axis, as evident from the subfigures 7(c)-(l). Further downstream, see subfigures 7(i)-(l) for $z = 2.5$ and $z = 3$ respectively, the flow field is dominated by vortices L1, H2 and by their symmetrical ones. Since their intensity is comparable, and since these 4 vortices are alternately counter-rotating, the flow maintains a configuration which is not symmetric. Nevertheless, the two flows coming from the two inlet pipes are definitely less mixed than in rectangular mixers, where only two co-rotating vortices are present which induce a strong convection between the two inlet fluids. Moreover, in the first part of the outlet pipe, approximately for $z \leq 1.0$, the in-plane velocity field remains almost symmetric with respect to the plane $x = 0$, and the flow coming from the the two inlet pipes remains separated, mixing being caused mainly by diffusion in this part of the channel. This aspect is well highlighted in figure 9, where the distribution of a passive scalar is reported at representative sections in the outlet pipe, together with representative streamlines of the secondary in-plane velocity vector aimed at highlighting convection due to secondary flow. In simulating the dynamics of the passive scalar, whose value is 0 or 1 depending on which inlet pipe is considered, a diffusion equal to $k = 3.0 \cdot 10^{-4}$ has been considered for numerical stability, thus limiting the observability of the separation between the two flows when we consider a section z which is too far from the confluence region. Nevertheless, the separation is quite sharp at least up to $z = 3$, which is the maximum value considered in figure 9. Subfigures 9, especially if considered sequentially for increasing values of z, show that convection, and the secondary flow in particular, plays a crucial role in the redistribution of the passive scalar in the z-sections. However, the mixing between the two flows coming from the two pipes remains moderate. The streamlines in subfigures 9 further confirm the analysis carried out on the basis of figure 7 on the vortex dynamics in the engulfment regime, showing that after some distance from the confluence region a four-vortices configuration is observed, where two vortices come from the RH region and

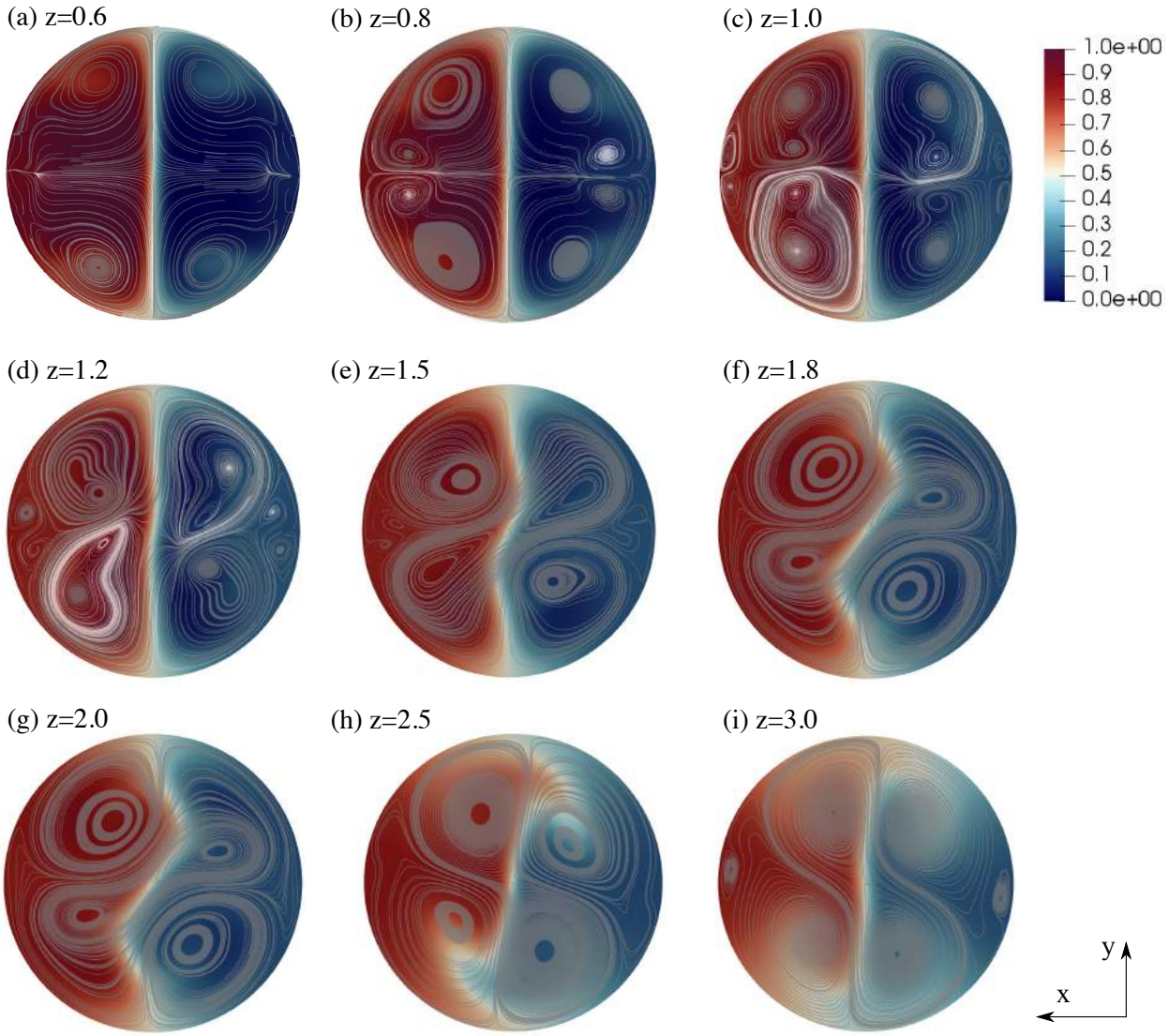

FIG. 9. Flow field in the engulfment regime at $Re = 550$: distribution of a passive scalar, whose value is 0 in one inlet pipe and 1 in the other, at different z sections in the outlet pipe from (a) z=0.6 to (i) z=3.0; streamlines of the secondary in-plane velocity vector are also reported.

two from the RL region. On each side, $x \geq 0$ and $x \leq 0$, two counter-rotating vortices are present, one coming from the RH and one from the RL region.

D. Stability analysis of the vortex regime

DNS simulations showed that for the CTM the engulfment regime is observed at $Re = 490$, whereas for $Re = 475$ the vortex regime is found and hysteresis in Re is absent as verified

by DNS (not shown here for brevity). The flow at $Re = 475$ was selected as baseflow for the stability analysis, in order to be as near as possible to the critical condition but still in the subcritical range.

As a first step, by using the Arnoldi-Krylov algorithm on the linearized version of the DNS code, the eigenvalue associated to the least stable mode was found to be slightly stable ($\sigma = -4.7 \cdot 10^{-2}$). The identified value is in agreement with the non-linear simulations as it indicates that for Re=475 the flow is almost marginally stable. Moreover, since the investigated instability is a pitchfork one, a real eigenvalue is consistent with the searched instability.

The critical Reynolds number is estimated by linearly extrapolating the value of Re such that $\lambda(Re) = 0$ considering two slightly subcritical cases at $Re = 450$ and $Re = 475$. By using the least stable eigenvalues found at $Re = 450$ ($\sigma = -2.45 \cdot 10^{-2}$) and at $Re = 475$ ($\sigma = -4.7 \cdot 10^{-2}$), the resulting critical Reynolds number for the circular section Re_{cr} is equal to $Re_{cr} \simeq 481$. The Re_{cr} estimated by linear stability analysis carried out by the matrix-method, i.e. with a numerical setup which is completely different from the one used for DNS, is thus in the range $[475 - 490]$ estimated with DNS simulations.

A further confirmation that the identified eigenmode is the one related to the instability leading to the engulfment regime has been obtained by comparing the perturbation field $\hat{\mathbf{u}}$ evaluated by DNS and the one obtained by linear stability, as depicted in Figure 10. The velocity components on the left column were evaluated by subtracting the flow in subcritical condition ($Re = 475$) from the postcritical one ($Re = 490$), i.e. solving equation (6) with respect to $\mathbf{u}$, while the ones on the right column were obtained through linear stability analysis, properly rescaled in amplitude for simplifying the comparison against DNS. As it can be seen from the comparison in figure 10, there is a good agreement between the least stable eigenmode and the perturbation field obtained by DNS, further confirming that the mode identified by the stability analysis is the one responsible for the onset of the observed engulfment regime.

V. CONCLUSIONS

The flow occurring in T-mixers made by pipes with circular cross section has been investigated here. Despite the simplicity of the geometry and the interest of the scientific

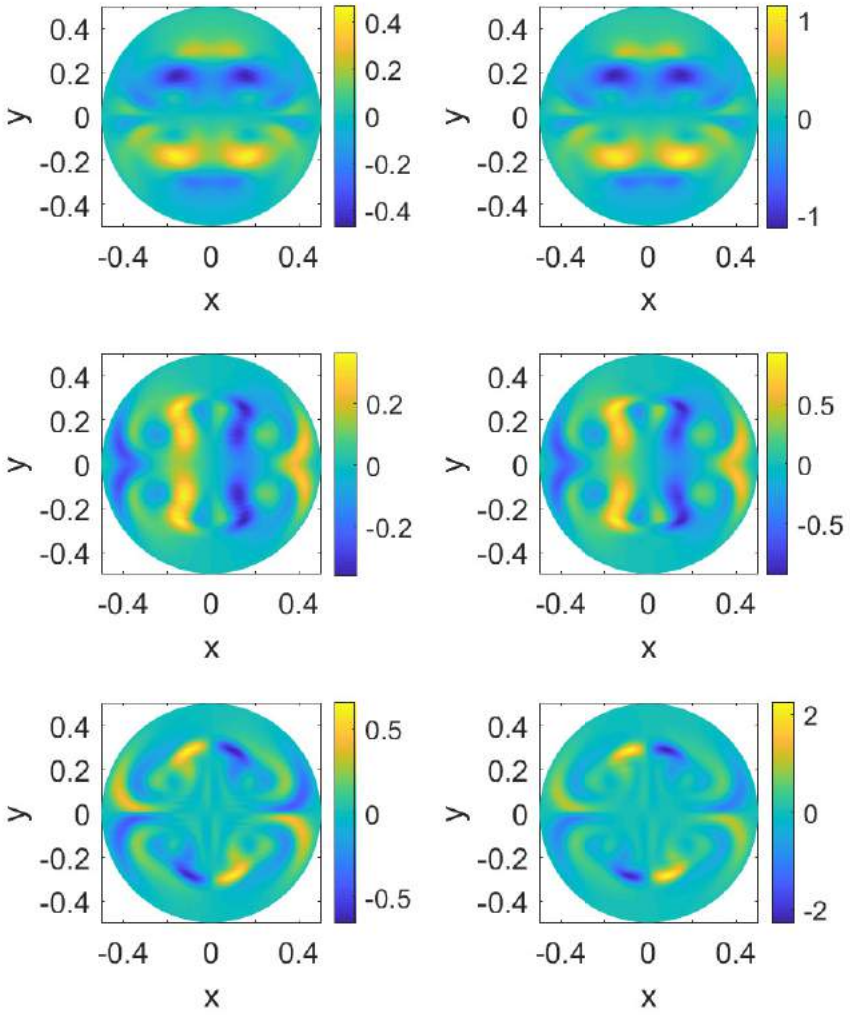

FIG. 10. CTM: comparison between perturbation field $\hat{\mathbf{u}}$ at z=2 obtained by DNS (left) and global linear stability (right); each row represents one velocity component, from the x-component on top to the z-component at the bottom.

community for T-mixers operating at low Reynolds numbers, to the authors' knowledge this kind of mixers has not been systematically investigated in the literature before. Conversely, several studies have been dedicated to investigate T-mixers made by channels with rectangular cross sections, and the corresponding flow features have been well characterized in the literature.

The present investigation is dedicated to study the characteristics of two regimes, i.e. the

vortex and the engulfment regimes. Both regimes are investigated by numerical simulation. The engulfment regime is the first one encountered, as Re is increased starting from low values, in which the flow does not respect the reflectional symmetries of the geometry (although both the geometry and the inflow conditions are symmetric). The vortex regime is the regime which precedes the engulfment in terms of Re, in which the flow has the same reflectional symmetries of the geometry. The two regimes and, in particular, the transition from one to the other, are generally important in T-mixers as engulfment leads to a substantial increase of mixing. The transition between the two regimes have been investigated here also by global stability analysis.

Results reported show that both the vortex and the engulfment regimes are substantially different in comparison to what happens for mixers with rectangular channels. Firstly, the occurrence of engulfment in circular T-mixers is observed at definitely larger values of Re (about 3.5 times larger considering the STM). Moreover, it is shown that the vortex regime in CTM is substantially different in comparison with the equivalent regime in rectangular mixers because the vortical structures which dominate the flow have different origin in the two cases. The difference between the two types of mixers is even more evident in the engulfment regime. In the engulfment regime in circular T-mixers the flow is only mildly asymmetric in contrast with rectangular ones and this is again caused by differences in the dominant vortical structures. In particular, it is shown that the flow characteristics in the circular case are dominated by the vortices forming at the curved edges at the intersection between the three pipes, and asymmetry of the flow is evident only in the outlet pipe, while in the inlet pipes and in the intersection region the flow practically maintains the reflectional symmetries of the geometry. As a result, mixing is not significantly increased in the engulfment regime in circular T-mixers, conversely to what observed for the rectangular ones. Finally, global stability analysis, combined with DNS, provides evidence that the instability leading the flow from the vortex to the engulfment regime is a supercritical pitchfork bifurcation.

ACKNOWLEDGEMENTS

The authors acknowledge the CINECA award under the ISCRA initiative, for the availability of high-performance computing resources and support.

DATA AVAILABILITY STATEMENT

The data that support the findings of this study are available from the corresponding author upon reasonable request.

REFERENCES

[1]N. T. Nguyen and Z. Wu, "Micromixers - A review," Journal of Micromechanics and Microengineering **15** (2005).

[2]G. Cai, L. Xue, H. Zhang, and J. Lin, "A review on micromixers," Micromachines **8** (2017).

[3]V. Hessel, H. Löwe, and F. Schönfeld, "Micromixers - A review on passive and active mixing principles," Chemical Engineering Science **60**, 2479–2501 (2005).

[4]C. Y. Lee, W. T. Wang, C. C. Liu, and L. M. Fu, "Passive mixers in microfluidic systems: A review," Chemical Engineering Journal **288**, 146–160 (2016).

[5]S. Camarri, A. Mariotti, C. Galletti, E. Brunazzi, R. Mauri, and M. V. Salvetti, "An Overview of Flow Features and Mixing in Micro T and Arrow Mixers," Industrial and Engineering Chemistry Research **59**, 3669–3686 (2020).

[6]I. Lashgari, O. Tammisola, V. Citro, M. P. Juniper, and L. Brandt, "The planar X-junction flow: Stability analysis and control," Journal of Fluid Mechanics **753**, 1–28 (2014).

[7]J. Zhang, W. Li, X. Xu, H. Liu, and F. Wang, "Experimental investigation of three-dimensional flow regimes in a cross-shaped reactor," Physics of Fluids **31** (2019).

[8]J. W. Zhang, T. Liang Yao, W. Feng Li, M. El Hassan, X. Lei Xu, H. Feng Liu, and F. Chen Wang, "Trapping region of impinging jets in a cross-shaped channel," AIChE Journal **66**, 1–9 (2020).

[9]M. Engler, N. Kockmann, T. Kiefer, and P. Woias, "Numerical and experimental investigations on liquid mixing in static micromixers," Chemical Engineering Journal **101**, 315–322 (2004).

[10]M. Hoffmann, M. Schlüter, and N. Räbiger, "Experimental investigation of liquid–liquid mixing in T-shaped micro-mixers using -LIF and -PIV," Chemical Engineering Science **61**, 2968–2976 (2006).

[11]D. Bothe, C. Stemich, and H. J. Warnecke, "Fluid mixing in a T-shaped micro-mixer," Chemical Engineering Science **61**, 2950–2958 (2006).

[12]D. Bothe, C. Stemich, and H. J. Warnecke, "Computation of scales and quality of mixing in a T-shaped microreactor," Computers and Chemical Engineering **32**, 108–114 (2008).

[13]S. Dreher, N. Kockmann, and P. Woias, "Characterization of Laminar Transient Flow Regimes and Mixing in T-shaped Micromixers," Heat Transfer Engineering **30**, 91–100 (2009).

[14]T. A. Ooms, R. Lindken, and J. Westerweel, "Digital holographic microscopy applied to measurement of a flow in a T-shaped micromixer," Experiments in Fluids **47**, 941–955 (2009).

[15]S. Thomas and T. a. Ameel, "An experimental investigation of moderate Reynolds number flow in a T-Channel," Experiments in Fluids **49**, 1231–1245 (2010).

[16]S. Thomas, T. Ameel, and J. Guilkey, "Mixing kinematics of moderate Reynolds number flows in a T-channel," Physics of Fluids **22**, 013601 (2010).

[17]N. Kockmann and D. M. Roberge, "Transitional flow and related transport phenomena in curved microchannels," Heat Transfer Engineering **32**, 595–608 (2011).

[18]T. Andreussi, C. Galletti, R. Mauri, S. Camarri, and M. V. Salvetti, "Flow regimes in T-shaped micro-mixers," Computers and Chemical Engineering **76**, 150–159 (2015).

[19]A. S. Lobasov, A. V. Minakov, and V. Y. Rudyak, "Viscosity effect on the flow patterns in T-type micromixers," Fluid Dynamics **51**, 381–388 (2016).

[20]A. S. Lobasov and A. V. Minakov, "Analyzing mixing quality in a T-shaped micromixer for different fluids properties through numerical simulation," Chemical Engineering and Processing: Process Intensification **124**, 11–23 (2018).

[21]M. A. Ansari, K. Y. Kim, K. Anwar, and S. M. Kim, "Vortex micro T-mixer with non-aligned inputs," Chemical Engineering Journal **181-182**, 846–850 (2012).

[22]L. Siconolfi, A. Fani, S. Camarri, and M. V. Salvetti, "Effect of geometry modifications on the engulfment in micromixers: Numerical simulations and stability analysis," European Journal of Mechanics, B/Fluids **55**, 360–366 (2016).

[23]A. Fani, S. Camarri, and M. V. Salvetti, "Investigation of the steady engulfment regime in a three-dimensional T-mixer," Physics of Fluids **25** (2013).

[24]A. Soleymani, H. Yousefi, and I. Turunen, "Dimensionless number for identification of flow patterns inside a T-micromixer," Chemical Engineering Science **63**, 5291–5297 (2008).

[25]C. Galletti, M. Roudgar, E. Brunazzi, and R. Mauri, "Effect of inlet conditions on the engulfment pattern in a T-shaped micro-mixer," Chemical Engineering Journal **185-186**, 300–313 (2012).

[26]R. Poole, M. Alfateh, and A. P. Gauntlett, "Bifurcation in a T-channel junction: Effects of aspect ratio and shear-thinning," Chemical Engineering Science **104**, 839–848 (2013).

[27]A. Mariotti, C. Galletti, R. Mauri, M. V. Salvetti, and E. Brunazzi, "Steady and unsteady regimes in a T-shaped micro-mixer: Synergic experimental and numerical investigation," Chemical Engineering Journal **341**, 414–431 (2018).

[28]A. Fani, S. Camarri, and M. V. Salvetti, "Unsteady asymmetric engulfment regime in a T-mixer," Physics of Fluids **26** (2014).

[29]J. W. Zhang, W. F. Li, X. L. Xu, M. El Hassan, H. F. Liu, and F. C. Wang, "Effect of geometry on engulfment flow regime in T-jet reactors," Chemical Engineering Journal **387** (2020).

[30]F. Giannetti, P. Luchini, and L. Marino, "Stability and Sensitivity Analysis of Non-Newtonian Flow through an Axisymmetric Expansion," Journal of Physics: Conference Series **318** (2011).

[31]E. Sanmiguel-Rojas and T. Mullin, "Finite-amplitude solutions in the flow through a sudden expansion in a circular pipe," Journal of Fluid Mechanics **691**, 201–213 (2011).

[32]S. Camarri, "Flow control design inspired by linear stability analysis," Acta Mechanica **226**, 979–1010 (2015).

[33]D. Fabre, V. Citro, D. F. Sabino, P. Bonnefis, J. Sierra, F. Giannetti, and M. Pigou, "A Practical Review on Linear and Nonlinear Global Approaches to Flow Instabilities," Applied Mechanics Reviews **70**, 1–16 (2018).

[34]L. Siconolfi, S. Camarri, and M. V. Salvetti, "T-mixer operating with water at different temperatures: Simulation and stability analysis," Physical Review Fluids **3**, 33902 (2018).

[35]E. Anderson, Z. Bai, C. Bischof, S. Blackford, J. Demmel, J. Dongarra, J. Du Croz, A. Greenbaum, S. Hammarling, A. McKenney, and D. Sorensen, *LAPACK Users' Guide*, 3rd ed. (Society for Industrial and Applied Mathematics, Philadelphia, PA, 1999).

[36]J. C. Loiseau, M. A. Bucci, S. Cherubini, and J. C. Robinet, "Time-stepping and Krylov methods for large-scale instability problems," Computational Methods in Applied Sciences **50**, 33–73 (2019), arXiv:1804.03859.

[37]J. Jeong and F. Hussain, "On the identification of a vortex," Journal of Fluid Mechanics **285**, 69–94 (1995).